NATIONAL AERONAUTICS AND SPACE ADMINISTRATION

Technical Report 32-1506

Mariner Mars 1969 SCAN Control Subsystem Design and Analysis

T. Kerner

H. H. Horiuchi

JET PROPULSION LABORATORY
CALIFORNIA INSTITUTE OF TECHNOLOGY
PASADENA, CALIFORNIA

October 30, 1970

NATIONAL AERONAUTICS AND SPACE ADMINISTRATION

Technical Report 32-1506

Mariner Mars 1969 SCAN Control Subsystem Design and Analysis

T. Kerner

H. H. Horiuchi

JET PROPULSION LABORATORY
CALIFORNIA INSTITUTE OF TECHNOLOGY
PASADENA, CALIFORNIA

October 30, 1970

Prepared Under Contract No. NAS 7-100
National Aeronautics and Space Administration

Preface

The work described in this report was performed by the Guidance and Control Division of the Jet Propulsion Laboratory.

Since the writing of the material in this report, the SCAN control subsystem has been built and successfully passed type approval testing and flown on the two *Mariner* Mars 1969 spacecraft. The subsystem performed satisfactorily during both spacecraft flights.

Contents

Tables

Figures

Contents (contd)

Figures (contd)

Abstract

The SCAN platform control system designed for the *Mariner* Mars 1969 spacecraft is described. The platform, which acts as a mounting base for the science instruments, has two deg-of-freedom about a set of spacecraft fixed coordinates. The system controls the platform movement and position. This report covers the detailed system design, the servo analysis, and the system error analysis.

Mariner Mars 1969 SCAN Control Subsystem Design and Analysis

I. Introduction

A. Background

The scientific experiments on the *Mariner* Mars 1969 spacecraft include a narrow-angle TV camera, a wide-angle TV camera, an infrared spectrometer, an infrared radiometer, and an ultraviolet spectrometer. These instruments are mounted on the SCAN platform.

The overall *Mariner* Mars 1969 spacecraft and SCAN platform configuration are shown in Fig. 1. Figure 2 illustrates a coordinate system convention used for specifying SCAN platform angles. As illustrated, the SCAN platform is a two-deg-of-freedom structure. The SCAN platform clock axis allows rotation of the platform about the Z axis of the spacecraft. The clock axis bearings are located in the center of the platform octagon structure. The platform clock angle is the angle between the projections in the spacecraft X-Y plane of the platform line-of-sight (LOS) and the Canopus tracker LOS; the platform LOS is defined as the line-of-sight of the narrow-angle television camera.

The SCAN platform cone axis allows rotation of the platform about a line in the X-Y plane; the cone angle is the angle between the platform LOS and the spacecraft $-Z$ axis. The cone axis bearings, platform structure, and platform mounted instruments are cantilever mounted from the spacecraft structure in the $+Z$ direction; this is the direction which is normally away from the sun.

The two-deg-of-freedom motion of the SCAN platform is servo controlled through the SCAN control system. The SCAN control system implements the SCAN platform pointing necessary to meet the *Mariner* Mars 1969 mission objectives.

This report presents a detailed description and comprehensive analysis of the *Mariner* Mars 1969 SCAN control system.

B. Functional Description

The *Mariner* Mars 1969 SCAN control system consists of the electromechanical and electronic devices necessary

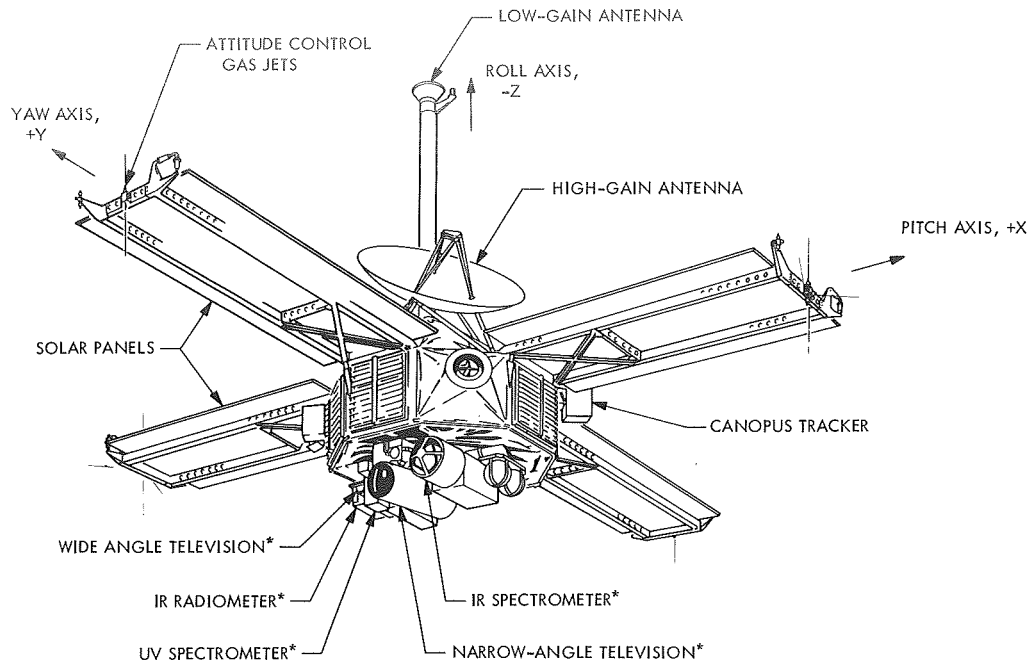

SCAN PLATFORM THERMAL BLANKET DELETED
*SCAN PLATFORM MOUNTED SCIENCE INSTRUMENTS

Fig. 1. *Mariner* Mars 1969 spacecraft

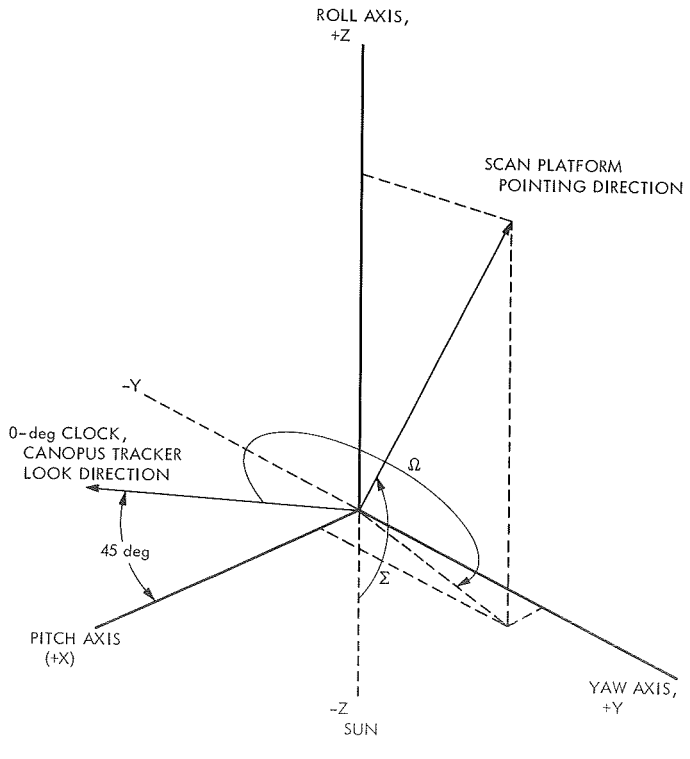

Σ SCAN PLATFORM CONE ANGLE
Ω SCAN PLATFORM CLOCK ANGLE

Fig. 2. SCAN platform system coordinate convention

to provide pointing control of the SCAN platform during the planetary encounter sequence. A functional block diagram of the SCAN control system is shown in Fig. 3; as shown in this block diagram, the servo mechanisms which are used to control the position of the planetary SCAN platform can be operated in two basic modes. In the first mode the servo error signals are obtained by a planet sensor. Since this planet sensor is mounted on the SCAN platform, closed-loop tracking of the planet is provided. In the second mode the servo error signals are obtained as the difference between a stored command signal (voltage) and the platform position as measured by the platform actuators. Therefore, the second mode provides open-loop platform pointing; i.e., the platform is pointed relative to the spacecraft orientation and not relative to the planet direction.

The first operating mode described above, closed-loop tracking of the center of brightness of the planet is used during the far-encounter (FE) mode. By definition, encounter E occurs at the time that the spacecraft makes its closest approach to the planet. Far-encounter nominally occurs between $E - 47$ h and $E - 12$ h. During this time a series of TV pictures are taken. The TV camera used for the FE phase has a field of view (FOV) of 1.1 × 1.4 deg. Closed-loop tracking of the planet using

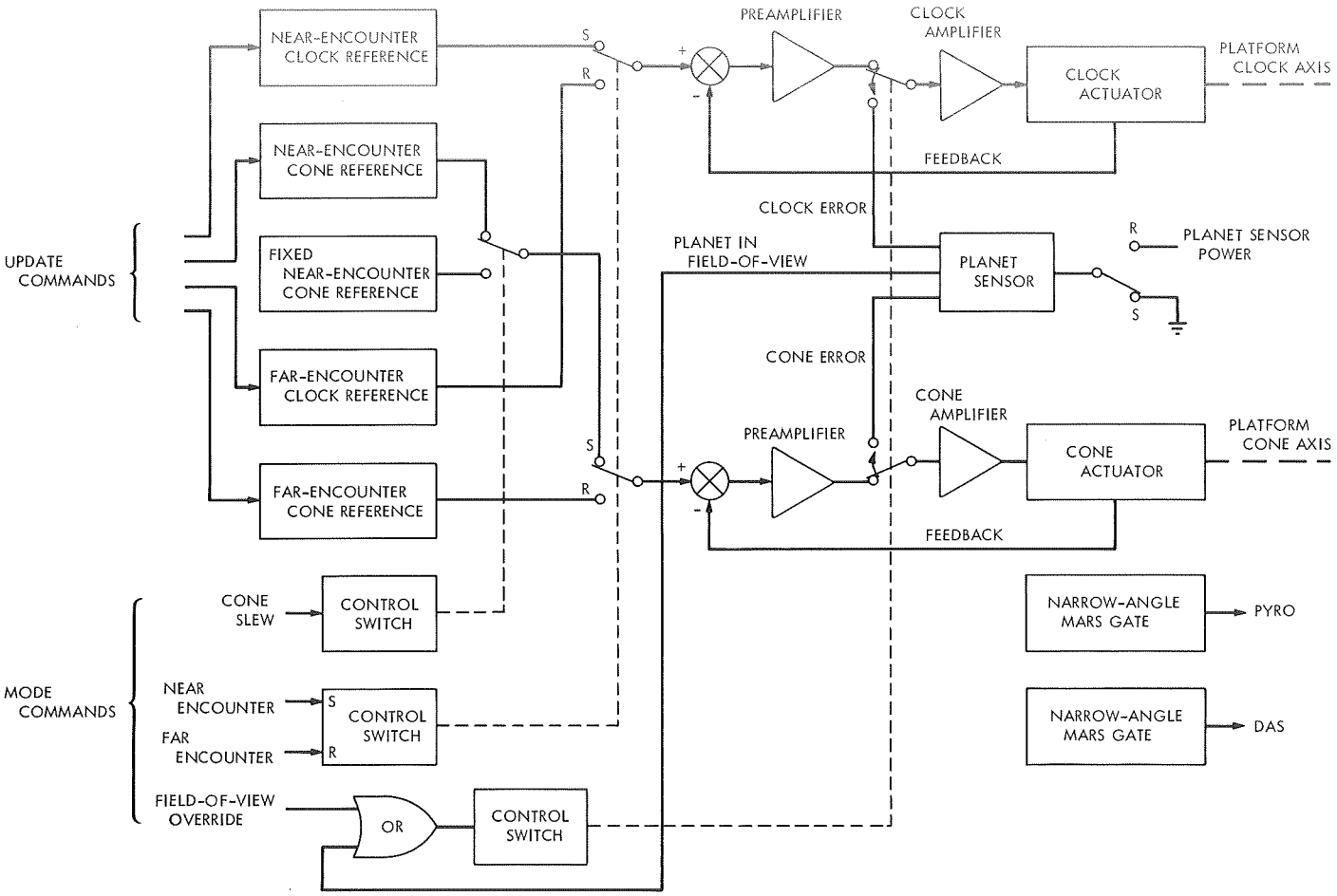

Fig. 3. SCAN control system functional block diagram

the planet sensor maintains the planet centered in the TV camera FOV during the *FE* sequence.

In the second operating mode described above, open-loop pointing of the platform line-of-view (relative to the spacecraft orientation) is used both during the *FE* and near-encounter (*NE*) modes. Open-loop pointing during *FE* is used to erect the platform to an initial pointing direction so that the planet is within the FOV of the planet sensor. A unique pointing direction, defined by the *FE* clock and cone reference angles of Fig. 3, is included in the mechanization of the SCAN control system for this purpose. Open-loop pointing of the platform during the *NE* sequence is used to establish and maintain a series of platform pointing directions. These pointing directions are chosen and sequenced to fulfill the pointing requirement of the various *Mariner* Mars 1969 experiments. The *NE* platform pointing is accomplished using the one variable *NE* clock reference angle and two (only one variable) *NE* cone reference angles shown in Fig. 3.

Included in the SCAN control system is a set of mode-control electronics. These mode-control electronics include all the logic and relays necessary to switch, either automatically or upon external command, from the stored open-loop pointing direction to the planet sensor, and to switch between the stored open-loop pointing directions. The primary features of the mode-control electronics are illustrated in Fig. 3; the relays are shown in a *NE* pointing mode in this block diagram.

Also a part of the *Mariner* Mars 1969 SCAN control system, and shown in Fig. 3, are two narrow-angle Mars gates (NAMG's). These NAMG's are optical sensors which are used to detect the planet in their FOV; they provide a level change output signal when the planet enters their FOV. The two NAMG's are used to initiate (1) cooldown of the infrared spectrometer, and (2) TV picture coverage during the planetary *NE* sequence. The NAMG's thereby provide automatic spacecraft operation and preclude the necessity for ground commands to initiate these functions.

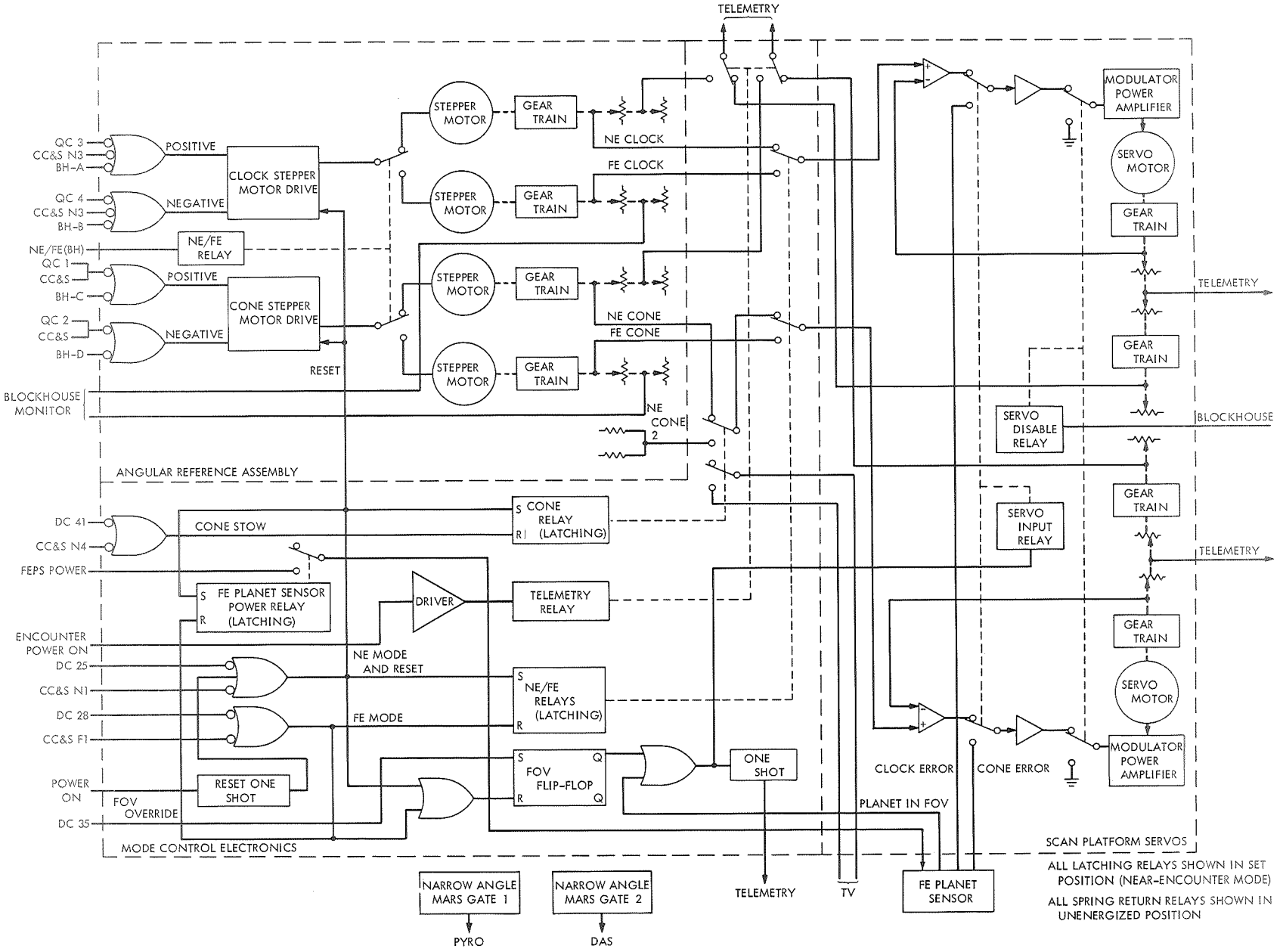

Fig. 4. SCAN control system detailed block diagram

II. SCAN Control System Design and Analyses

The SCAN control system is logically discussed in terms of its five major functional parts, as follows:

(1) Angular reference assembly.

(2) Mode control electronics.

(3) Platform servos.

(4) Planet sensor.

(5) Narrow-angle Mars gates.

These five parts are identified in the detailed block diagram in Fig. 4. The description of the system detailed design and critical analyses in this section of this report are also organized according to the five functional parts listed above.

A. SCAN Angle Reference and Operational Modes

1. Angular reference assembly. As shown in Fig. 4, the angular reference assembly consists of four stepper motor-gear train-potentiometer subassemblies used as variable storage elements for platform pointing angles; one each *NE* clock, *FE* clock, *NE* cone, and *FE* cone pointing angles are stored. In addition, a voltage divider network provides an output voltage representing a second, fixed, *NE* cone pointing angle. The electronic circuits and switching logic included as part of the angular reference assembly provide the drive signals required to move the stepper motor subassemblies to comply with the angular command inputs.

a. Pulse-sum-to-analog converters. Four stepper motor-gear train-potentiometer subassemblies, more commonly called pulse-sum-to-analog converters, are used in the angular reference assembly. The four subassemblies are identical. A schematic diagram representation of one subassembly and a manufactured converter subassembly are shown in Figs. 5 and 6, respectively.

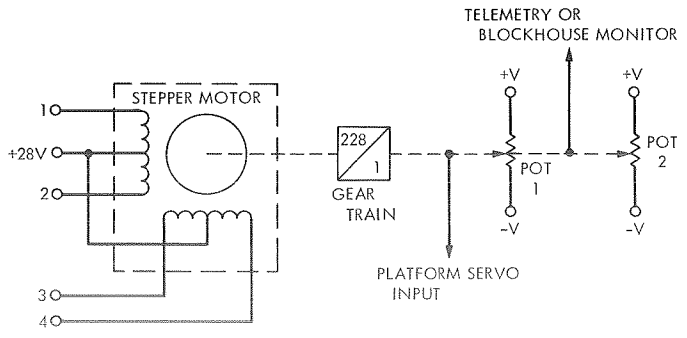

Fig. 5. Pulse-sum-to-analog converter block diagram

Potentiometer 1 in Fig. 5 is used to provide the reference input to the SCAN platform servos. This potentiometer is identical to the potentiometers used in the platform actuators for position feedback. The commanded platform angle is, therefore, proportional to the position of this potentiometer. The resistive element in this potentiometer is a plastic film which provides very high resolution. This type of potentiometer was chosen for its low-noise characteristics.

Potentiometer 2 in Fig. 5 is used to monitor the angular position stored in the assembly. As shown in Fig. 4, the monitoring is accomplished through telemetry channels on the *NE* clock and cone angles and through blockhouse monitor lines on the *FE* clock and cone angles. The stored *NE* angles can be updated during flight while the stored *FE* angles can only be changed before launch.

The stepper motor is a 28 V, size 8 device which moves 90 deg per step. Referring to Fig. 5, sequential grounding of pins 4, 2, 3, and 1 will cause clockwise motor rotation; sequential grounding of pins 3, 2, 4, and 1 will cause counterclockwise motor rotation.

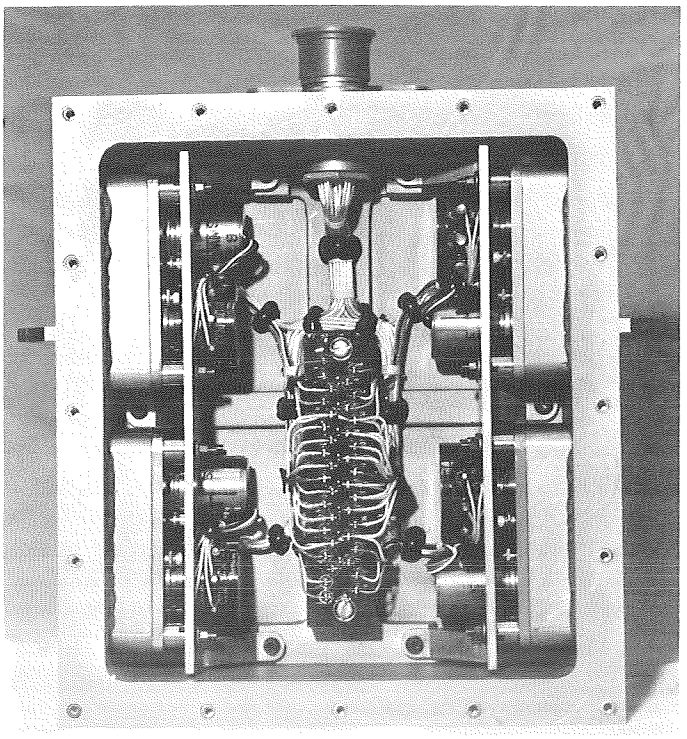

Fig. 6. Pulse-sum-to-analog converter subassembly

Since the stepper motor requires sequential energizing of four windings to rotate in a specific direction, it was decided to operate the stepper motor subassemblies so that they always rotate a multiple of 360 deg (either clockwise or counter-clockwise) and stop in a single, unique, rest position. The gear train was then selected to provide a scale factor of 1 deg of scan platform gimbal rotation for 360 deg of stepper motor rotation. Since both actuator feedback potentiometers are geared at a ratio of 1.58:1 compared to the platform axes, the desired scale factor requires a reduction of about 228:1 between the stepper motor and the potentiometer.

Alternately, it would have been possible to operate the stepper motors so that the required gimbal-motion resolution of 1 deg was represented by either 90 or 180 deg of stepper motor rotation. These modes of operation, however, would necessitate building a memory of the stepper motor-rotor orientation into the drive electronics so the proper winding could be selected to execute any given command. The mechanization of such a memory, which would have to operate over power transients, was judged undesirable.

b. Stepper motor-drive electronics. The stepper motor-drive electronics contain the logic and switching circuits necessary to interface between the angular command lines and the stepper motor subassemblies. The angular command lines which provide inputs to the stepper motor-drive electronics are shown in Fig. 4. The functional requirements fulfilled by these command lines are listed below:

(1) The stored *NE* clock and cone angle must be capable of being changed during flight through commands from either the Central Computer and Sequencer (CC&S) or Flight Command Subsystem (FCS).

(2) All angles stored on the stepper motor-driven subassemblies shall be capable of being changed and monitored for proper operation while on the launch pad.

The angular commands are sent as pulse trains. Each pulse commands an incremental change of 1 deg in the stored platform pointing direction. The stepper motors are operated so that a 360-deg rotation represents a 1-deg change in the stored pointing direction. Hence, since the stepper motors move in 90-deg steps for each winding actuation, a sequence of four stepper motor-winding actuations is necessary for each input command pulse.

A detailed logic diagram of the clock-axis stepper motor-drive electronics is shown in Fig. 7. The input command pulses are actually momentary circuit closures. These input lines are all held at a logical 1 ("high" voltage) except when the circuit is closed, as shown in Fig. 7. The input logic inverts these input commands and combines them in logical OR functions. Typical signals (A, B, and C) are shown in the timing diagram of Fig. 8.

The logical OR of all the input commands is transmitted to a noise discrimination circuit, consisting of a monostable, one shot, and a bistable flip-flop. This noise discrimination circuit provides noise rejection and also rejects any contact bounce on the command inputs by insuring that the stepper motor-drive electronics are triggered on the trailing edge of the command inputs. The operation of this circuit is illustrated in detail in the timing diagram of Fig. 9. The OR of the input commands is used to trigger the monostable, which is set for a nominal 15-ms pulse width. This monostable is ac triggered on the leading (rising) edge of the input pulse. The output of the monostable is connected to the ac-coupled clock input of a flip-flop. The flip-flop is triggered on the trailing (falling) edge of the monostable output. If the pulse which triggered the monostable is still present at the end of the 15-ms delay time, the flip-flop is set through the clocked set input and the remainder of the circuit action is enabled. If the input command has disappeared, valid inputs have a minimum pulse width of 75 ms, the flip-flop is clamped in the reset state through the direct reset input and the clocked set input is no longer enabled. Hence, the flip-flop does not change state when the clock input is triggered. The noise discrimination logic, therefore, discriminates against any input with a pulse width less than 15 ms and accepts any input with a pulse width greater than 15 ms.

The output of the noise discrimination logic is used to initiate the operation of the pulse generating logic. This pulse generating logic uses two ac-triggered monostables and associated control logic to generate the required sequence of four output pulses. A timing diagram for the pulse generating logic is presented in lines E thru K of Fig. 8. The first monostable is triggered for the first time when the flip-flop in the noise discrimination logic is reset. This monostable is set at a nominal pulse width of 65–70 ms. The input to this monostable is transmitted to the counting logic and the output, line F of Fig. 8, is transmitted to the second monostable. The second monostable, set at a nominal pulse width of 35 ms, is triggered on the trailing edge of signal F. The first three output

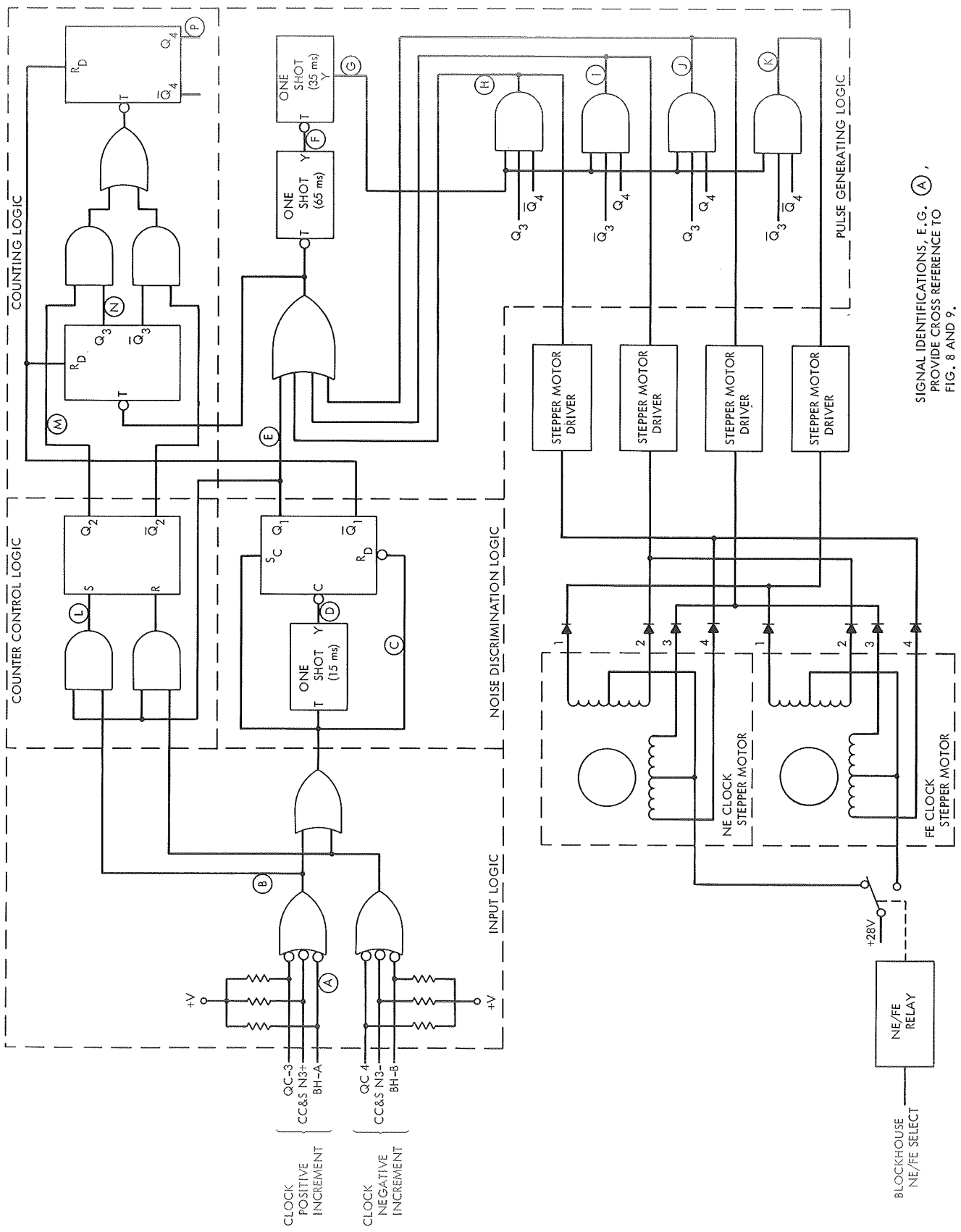

Fig. 7. Clock axis stepper motor-drive electronics logic diagram

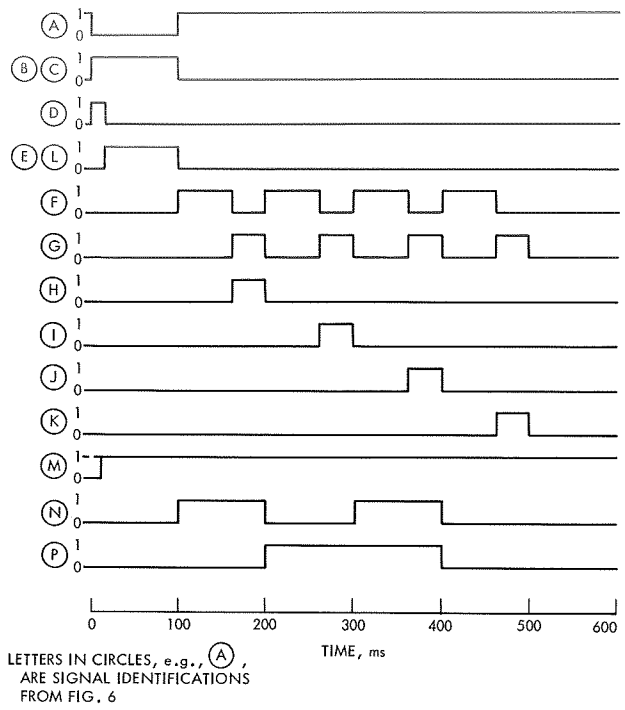

Fig. 8. Stepper motor-drive electronics timing diagram

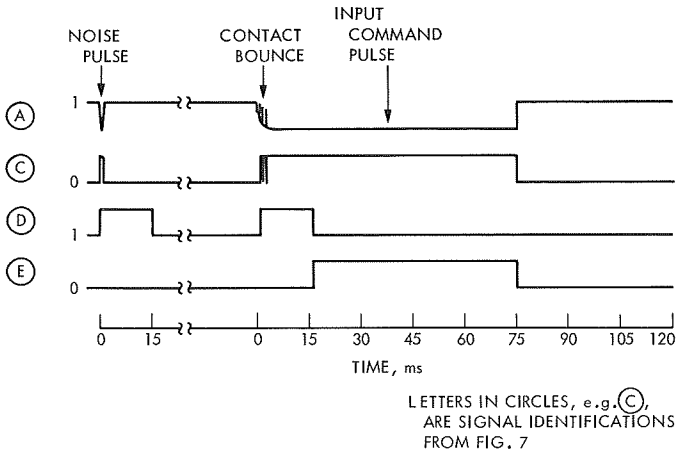

Fig. 9. Noise discrimination logic timing diagram

pulses from this second monostable are returned to the input of the first monostable through counter-controlled gates, signals H, I, J, where they retrigger this monostable. The same three pulses are also transmitted to the stepper motor-drive circuits. The fourth output pulse of the 35-ms monostable is transmitted only to the appropriate stepper motor-drive circuit. The pulse generating logic, therefore, generates a sequence of four output pulses to the stepper motor-drive circuits. The sequence of the pulses is controlled so that the stepper motor rotates through 360 deg in either a clockwise or counterclockwise direction.

The counter control logic contains a single flip-flop and a pair of AND gates. It receives as inputs the output from the noise discrimination logic and the input command pulse. The flip-flop is, therefore, set in the desired state 15 ms after an input command is received. The state of this flip-flop controls the sequence in which the counting logic operates and, therefore, the direction in which the stepper motor moves.

The counting logic contains two ac-triggered toggle flip-flops and associated control gates. The toggle input to this counter is the pulse input to the 65-ms one shot in the pulse generating logic. The first flip-flop Q_3 in the counting logic changes state with every input pulse. The second flip-flop Q_4 changes state as a function of the state of the first flip-flop and the flip-flop in the counter control logic. The two counting sequences are shown in Table 1.

Table 1. Counting logic sequences

Input pulse	Sequence 1	Sequence 2
1	10	11
2	01	01
3	11	10
4	00	00

The rest state of the counter is with both flip-flops reset. The output of the two flip-flops is used to control the recirculating gates in the pulse generating logic. A reset line is included in the logic to set these two flip-flops into the reset state. The reset line is energized by the introduction of each new pulse input to ensure a proper initial state on the counter flip-flops. The remainder of the logic in the stepper motor-drive electronics automatically assumes the correct quiescent logic condition.

The stepper motor drivers provide the power handling capability necessary to energize the stepper motor windings. These drivers sequentially ground the four output lines in the proper sequence to command one complete revolution of a stepper motor in the selected direction.

The +28-V stepper motor power is connected to the winding center taps through a *NE/FE* relay. The state of this relay is controlled through blockhouse lines. After launch, the relay is not energized and remains in the state shown in Fig. 7. Power is then supplied only to the *NE* stepper motors. A plan view of clock and cone drive logic and driver circuits is shown in Fig. 10.

A set of eight diodes is included between the drivers and the stepper motor windings. These diodes block the sneak current paths between the interconnected *NE* and *FE* stepper motors. Also included in the stepper motor-drive circuits, but not shown in Fig. 7, are suppression diodes to protect the drive circuits while switching the inductive motor windings.

2. *Mode-control electronics.* The SCAN control system mode-control electronics contain all the logic and switching functions necessary to implement the various operating modes and conditions of the system. The mode-control electronics accept a total of seven command signals from other subsystems and three logic control or switching functions generated within the SCAN control system. These control signals are all listed in Table 2.

A detailed block diagram of the SCAN mode-control electronics is included as part of Fig. 4. As illustrated, the mode-control electronics implement the following switching and control functions:

(1) Upon receipt of a *NE* mode command (CC&S N1 or DC-25), the *NE* clock and cone reference angles are connected to the inputs of SCAN platform servos.

(2) Upon receipt of a cone slew command CC&S N4 or DC-41, and while in the *NE* mode, the cone servo input is transferred to the fixed *NE* cone reference angle, and a relay closure is provided to the TV system.

(3) Upon receipt of a *FE* mode command CC&S F1 or DC-28, the *FE* clock and cone reference angles are connected to the inputs of SCAN platform servos, and power is applied to the planet sensor.

(4) Upon receipt of either a planet-in-field-of-view signal from the planet sensor or a field-of-view override command DC-35; while in the *FE* mode, a relay drive signal which is used to transfer the SCAN platform servo inputs from the *FE* angular references to the planet sensor is provided. Coincident with the transfer from angular reference to planet sensor, a one shot output is transmitted to a telemetry event recording channel.

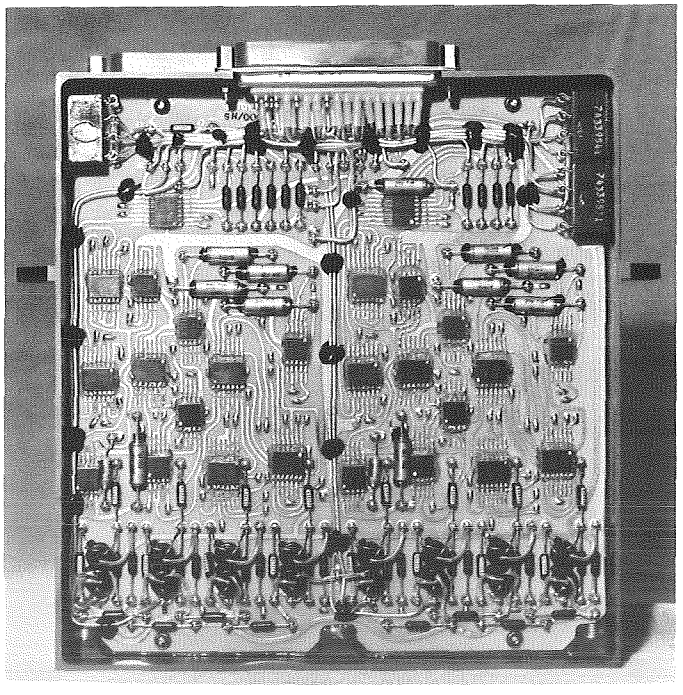

Fig. 10. SCAN platform drive logic electronics subassembly

Table 2. SCAN control system mode and switching inputs

Inputs from other systems	
Command	**Command function**
CC&S N1	Primary *NE* mode command
CC&S F1	Primary *FE* mode command
CC&S N4	Primary *NE* cone slew command
DC-25	Backup *NE* mode command
DC-28	Backup *FE* mode command
DC-41	Backup *NE* cone slew command
DC-35	Backup to automatic planet-in-field-of-view switching
Internally generated switching controls	
Command	**Command function**
Planet-in-field-of-view	Switches platform servos between planet sensor and angular references
Continuous power ON	Used to generate reset pulse to control subsystem logic initial conditions
Encounter power ON	Used to switch two telemetry lines from *NE* angular references to platform multispeed position readout

(5) When the encounter power is applied to the SCAN control system, nominally coincident with CC&S N1, two telemetry lines are transferred from the *NE* angular references to the platform multispeed readouts.

The hardware mechanization of the SCAN mode control electronics corresponds directly to the block diagram of Fig. 4 except for a switching inhibit which is part of the servo input-relay drive circuit. A logic diagram of this switching inhibit is shown in Fig. 11 as well as the circuit action of this switching inhibit. The switching inhibit is required because of the manner in which the planet-in-field-of-view signal is mechanized in the planet sensor; this signal is a logical 0 when the planet is out of the field-of-view, a logical 1 when the planet is in the field-of-view, and a logical 1 when the planet sensor power is OFF (lines 4 and 5 of Fig. 11). A logical interlock using a set of relay contacts from one of the *NE/FE* relays is, therefore, necessary to prevent transfer of the servo input relay to the *FE* planet sensor inputs while the SCAN control system is in the *NE* mode; this interlock is represented by signal 3 in Fig. 11. A second switching interlock which prevents transfer of the servo input relay during the period of time the *FE* mode command exists, nominally 100 ms, is also included in the electronics. This second switching interlock, signals 1 and 2 of Fig. 11, prevents momentary transfer of the servo input relay caused by the race between signals 3 and 5 when a *FE* mode command is received. Such a momentary transfer would not cause incorrect operation of the SCAN control system, but would trigger the one shot shown in Fig. 11 and cause an incorrect telemetry output.

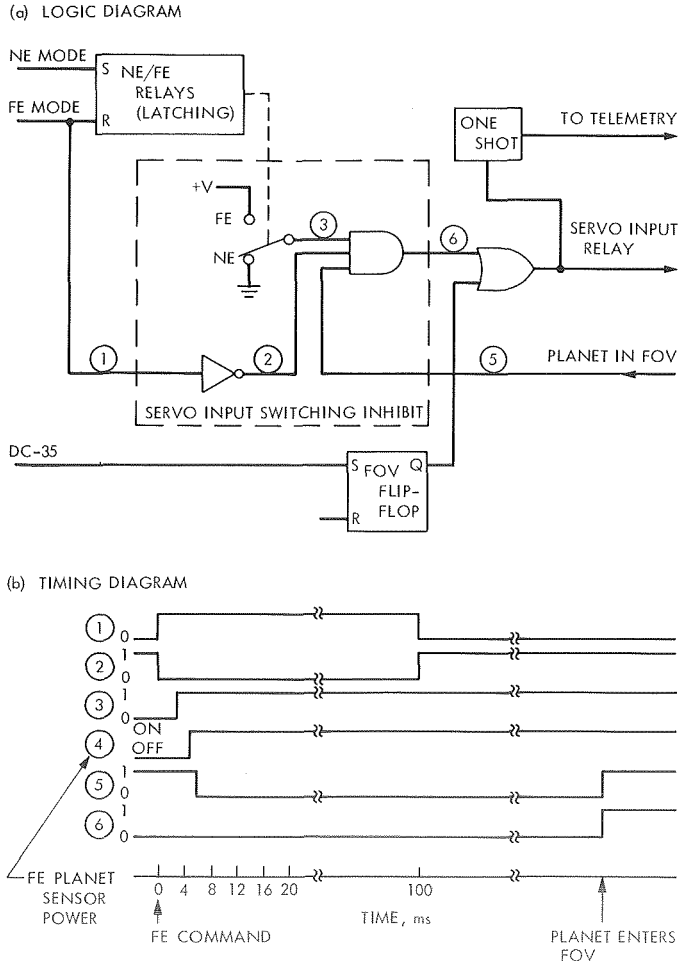

Fig. 11. Servo input switching inhibit

B. SCAN Platform Servos

The SCAN platform servos contain the control elements necessary to provide two-axis control of the SCAN platform. The servos include servo electronics and platform actuators for both the clock axis and the cone axis. An overall block diagram for the SCAN platform servos is shown in Fig. 4.

1. SCAN servo mathematical model. The only unusual problems associated with developing a mathematical model for the SCAN servo involves the representation of the actuator assembly and spacecraft structure. Both the linear and non-linear aspects of the servo motor, gear train, platform bearings, and flexible spacecraft elements must be considered. For this analysis, linear or linearized models are assumed.

The assumed single-axis linear model for the actuator and platform structure is shown in Fig. 12. The torsional coupling element shown represents the effective combination of all torsional elements coupling the actuator

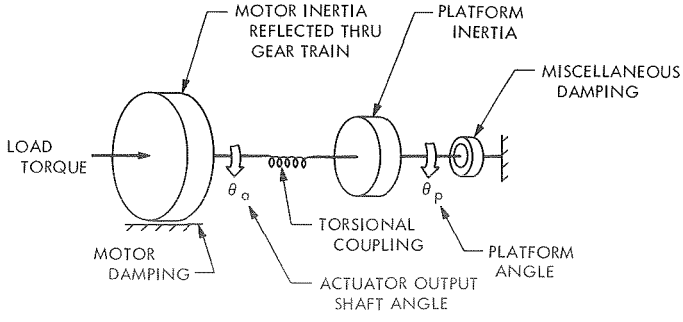

Fig. 12. SCAN control motor and platform rotational system model

to the platform. In the clock axis, this torsional element includes the spider which supports the clock actuator output shaft and gearing, the clock axis torque tube, the actuator-to-torque tube link, and any platform clock axis flexure. In the cone axis, the same elements except the spider and torque tube contribute to the torsional coupling. The approximate parameters associated with these torsional elements, and the calculated combined clock and cone axis spring constants are listed in Table 3.

The equations of motion for the rotational model of Fig. 12 are:

$$T_L = \alpha T_m = \alpha^2 J_m \ddot{\theta}_a + \alpha B_m \dot{\theta}_a + \kappa_p(\theta_a - \theta_p) \quad (1)$$

$$0 = J_p \ddot{\theta}_p + B_p \dot{\theta}_p + \kappa_p(\theta_p - \theta_a) \quad (2)$$

where

α = actuator gear ratio

T_m = servo motor torque

J_m = moment of inertia of servo motor rotor

B_m = servo motor damping constant

κ_p = spring constant of torsional coupling element

J_p = platform moment of inertia

B_p = miscellaneous platform damping

T_L = load torque

θ_a = actuator output shaft angle

θ_p = platform angle

Substituting Eq. (2) into Eq. (1),

$$\alpha T_m = \alpha^2 J_m \ddot{\theta}_a + \alpha B_m \dot{\theta}_a + J_p \ddot{\theta}_p + B_p \dot{\theta}_p \quad (3)$$

In this equation, $\alpha^2 J_m >> J_p$ and $\alpha B_m >> B_p$. Also, the bandwidth of the control servo will be maintained significantly less than the structural resonant frequency. The above equation may then be approximated by

$$\alpha T_m \cong \ddot{\theta}_a(\alpha^2 J_m + J_p) + \dot{\theta}_a(\alpha B_m + B_p).$$

The resultant simplified single-axis motor and load mathematical model is, therefore:

$$\alpha T_m = \ddot{\theta}_a(\alpha^2 J_m + J_p) + \dot{\theta}_a(\alpha B_m + B_p)$$

Table 3. Estimated SCAN structural resonance parameters

Spring constants	Parameters, ft-lb/rad
Clock torque tube	1.2×10^5
Clock axis spider	1.4×10^5
Actuator	2×10^4
Actuator-to-torque tube link	3.7×10^4
Platform clock axis	negligible
Platform cone axis	negligible
Total clock axis	1.08×10^4
Total cone axis	1.30×10^4
Moments of inertia	**Parameters, slug-ft^2**
Clock axis	
145-deg cone angle	4.2
155 deg	4.4
165 deg	4.9
Cone axis	5.4
Undamped natural frequency	**Parameters, Hz**
Clock axis	8.1
Cone axis	7.8

and

$$\theta_a = \frac{J_p}{\kappa_p}\ddot{\theta}_p + \frac{B_p}{\kappa_p}\dot{\theta}_p + \theta_p = \frac{\ddot{\theta}_p}{\omega_n^2} + \frac{2p}{\omega_n}\dot{\theta}_p + \theta_p \quad (4)$$

This is the model which is assumed for the SCAN control system linear servo block diagram of Fig. 13; a Laplace transform representation is assumed.

Other than the actuator model and platform dynamics, perhaps the least obvious feature of the SCAN servo model in Fig. 13 is the sine of the cone angle multiplier term in the planet sensor feedback for the clock axis. This term arises from the fact that the non-cone planet sensor error axis is not parallel with the clock axis, but rather is a cross-cone angle about an axis normal to the cone axis and to the platform line of sight. Hence, the sine of the cone angle term represents the coupling between the platform clock axis and the planet sensor cone axis.

The remaining elements in the block diagram in Fig. 13 consist of gains K_1 thru K_5, and shaping networks $G_1(S)$ and $G_2(S)$.

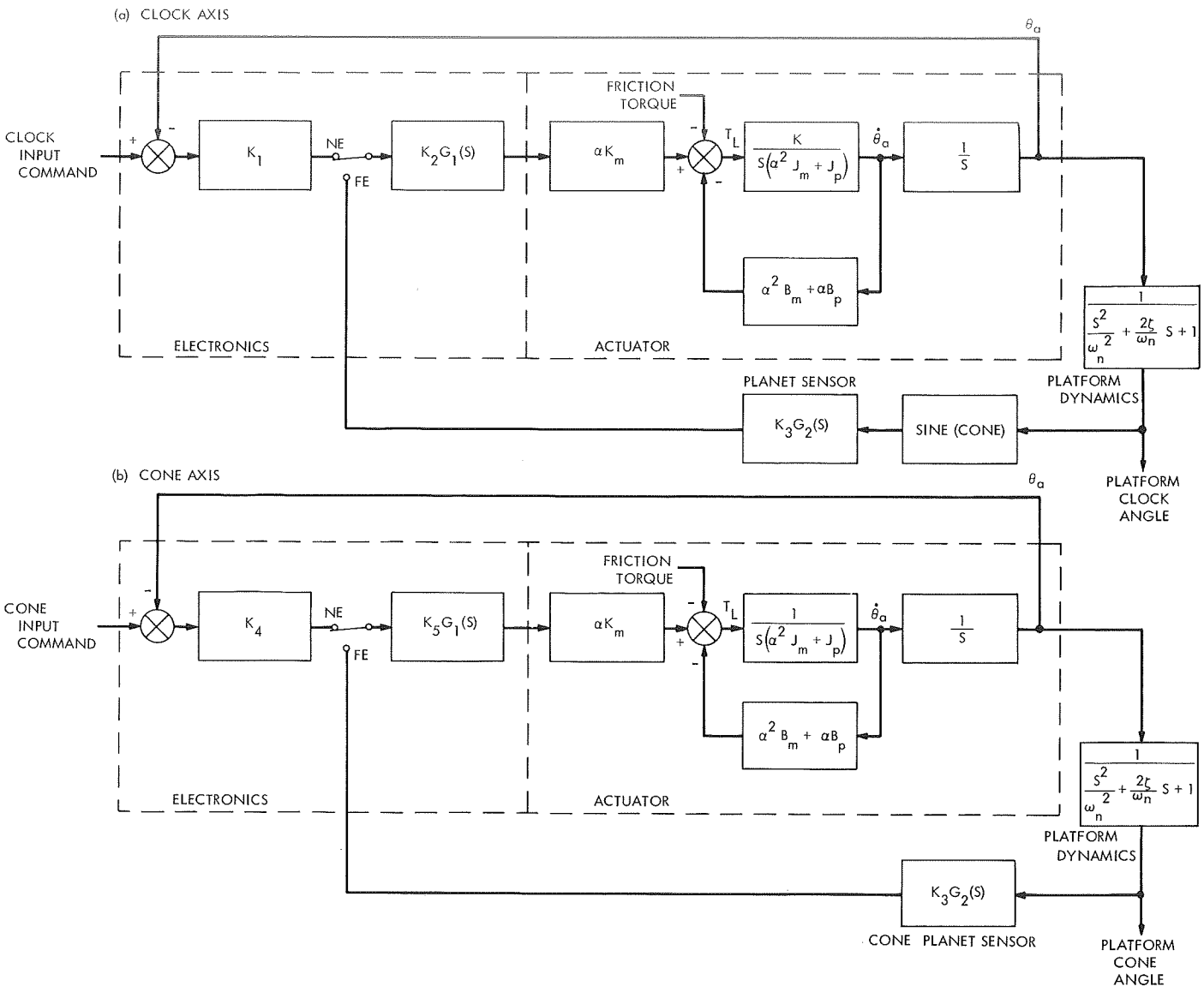

Fig. 13. SCAN control system linear servo block diagram

2. SCAN platform actuators. The two platform actuator subassemblies were designed to be identical. Each actuator subassembly consists of a servo motor, a series of gear trains, a slip clutch, and three potentiometers. The entire assembly is housed in a sealed, pressurized container. A schematic diagram of an actuator subassembly is shown in Fig. 14.

The major functional requirements for the SCAN platform actuators are listed below:

(1) The maximum platform angular rate (slewing speed) shall be greater than 1 deg/s.

(2) The actuator must hold the platform stationary during the thrust phase of the midcourse trajectory correction maneuver.

(3) The actuators must provide readout of platform clock and cone pointing directions with an accuracy of at least ± 0.2 deg per axis.

The servo motor was selected by considering the specified platform angular rate and the estimated platform loading. The bearing friction loads on the platform were estimated as about 20 in.-lb in a zero-g environment and 75–100 in.-lb in a 1-g environment. Driving these loads at a 1-deg/s rate requires 0.04 W, zero g, or

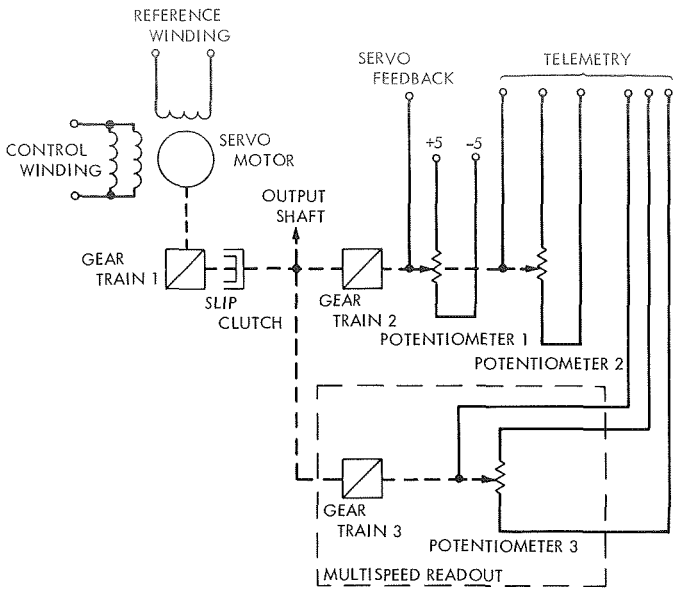

Fig. 14. SCAN platform actuator subassembly block diagram representation

0.2 W, 1 g, of mechanical power out of the actuator. Allowing a reasonable margin of safety for gear train inefficiencies, offset center-of-gravity loading in a 1-g environment, and errors in the loading estimates, it was decided that the servo motor should be capable of producing between 0.5 and 1.0 W of mechanical output power. These considerations led to the selection of a size 11, 400-cycle servo motor with the characteristics listed in Table 4.

Gear train 1 couples the motor to the output shaft of the actuator. This gear train includes a worm gear which holds the platform stationary against offset center-of-gravity torques during the thrust period of midcourse corrections, thereby satisfying the second functional requirement previously listed. The gear-train worm gear, however, limits the torque transmission efficiency of this gear train to about 50% max.

The gear ratio of this power transmitting gear train in the actuator may be selected by considering the servo-motor torque-speed characteristic. This characteristic, referred to the actuator output shaft, is:

$$T_L = \alpha K_T K_m V_r - (\alpha^2 B_m K_T + B_p)\,\dot{\theta}_a$$

where

K_T = gear train torque transmission efficiency

$$K_m = \frac{\text{motor stall torque}}{\text{motor rated voltage}} = 3.44 \times 10^{-3}\ \frac{\text{in.-lb}}{\text{V rms}}$$

$$B_m = \frac{\text{motor stall torque}}{\text{motor no load speed}} = 8.18 \times 10^{-7}\ \frac{\text{in.-lb}}{\text{deg/s}}$$

$B_p \cong 0$

$\dot{\theta}_a$ = angular rate of actuator output shaft

V_r = motor (control winding) rated voltage = 10 V rms

Assuming a nominal K_T of 40%, the linearized actuator speed–torque performance for several different gear ratios is presented in Fig. 15. From this analysis, a nominal gear ratio of about 27,000:1 was selected as providing adequate margins for both stall torque and slewing speed requirements.

The slip clutch shown in Fig. 14 is included in the actuator subassembly primarily to prevent damage to the gear train by transmitting excessive torque. The slip clutch is physically located one state of gearing away from the actuator output shaft, and is set at an equivalent output shaft torque of about 300 in.-lb.

Table 4. SCAN servo-motor characteristics

Characteristics	Minimum	Nominal
Stall torque, in.-oz	0.50	0.55
No load speed, rev/min	6500	7000
Rotor inertia, gm-cm^2		0.76
Input power, W/ϕ		3.5

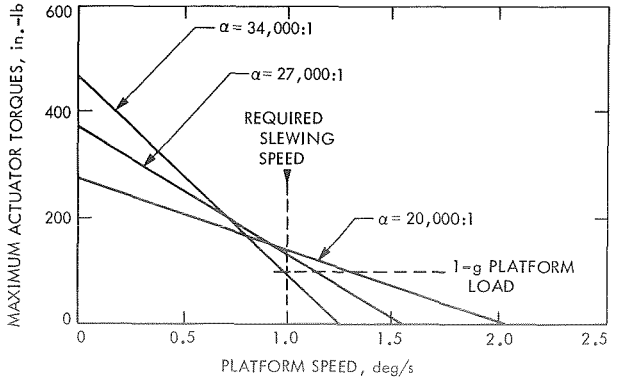

Fig. 15. SCAN actuator speed-torque characteristics

Gear train 2 provides a multiplication of 1.58 to 1 from the platform angle to the angle at potentiometers 1 and 2. This gear train is used so that the maximum actuator range (±108 deg) uses most of the available active angle on the potentiometers (±175 deg), thereby improving the accuracy and sensitivity of the platform servos. The gear train uses anti-backlash gears to limit errors in this loop. Potentiometer 1 is the servo feedback potentiometer. Potentiometer 2 is used for telemetry readout of the platform clock and cone angles. The accuracy of the platform angular readout from potentiometer 2 is limited by the telemetry channel encoding resolution of 1 in 127 parts to about ±0.85 deg.

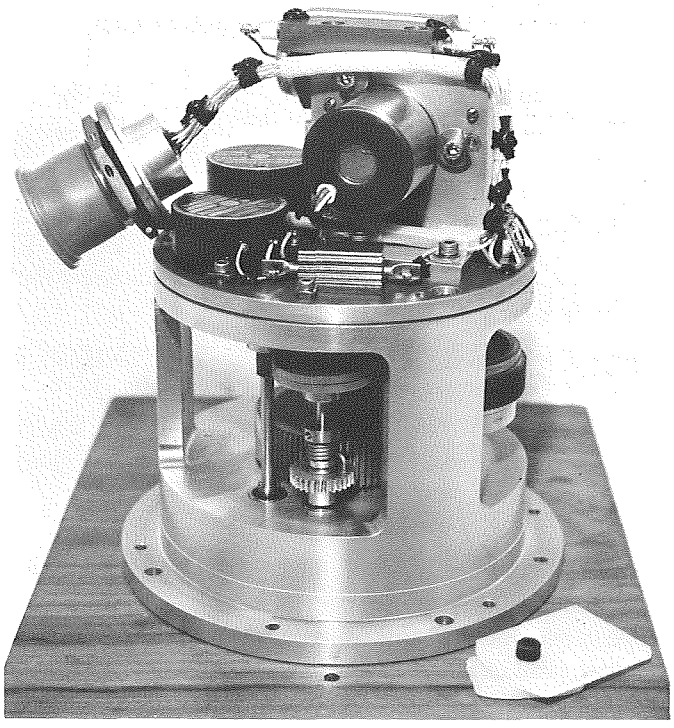

Fig. 16. SCAN platform drive actuator subassembly

The third actuator functional requirement in the previous list is satisfied by including gear train 3 and potentiometer 3 in the actuator mechanization. This gear train and potentiometer provide a multispeed platform position readout signal to the telemetry system. The gear ratio of gear train 3 is 79.25:1 and was selected so that no ambiguity from the single speed readout would exist in decoding the platform position readouts; it also would provide the necessary accuracy. The encoding resolution of 1 part in 127 for this multispeed readout provides a resolution in platform readout angle of approximately ±0.018 deg. Anti-backlash gearing is again employed to limit the errors in this gear train. Figure 16 shows the assembly of a scan servo actuator.

3. SCAN control system servo analysis. The linear SCAN control system model shown in Fig. 13 was used to design the SCAN servos and analyze the performance and stability margins to be associated with this control system. A single axis representation of this model, with several modifications to improve the accuracy of the analysis, is shown in Fig. 17.

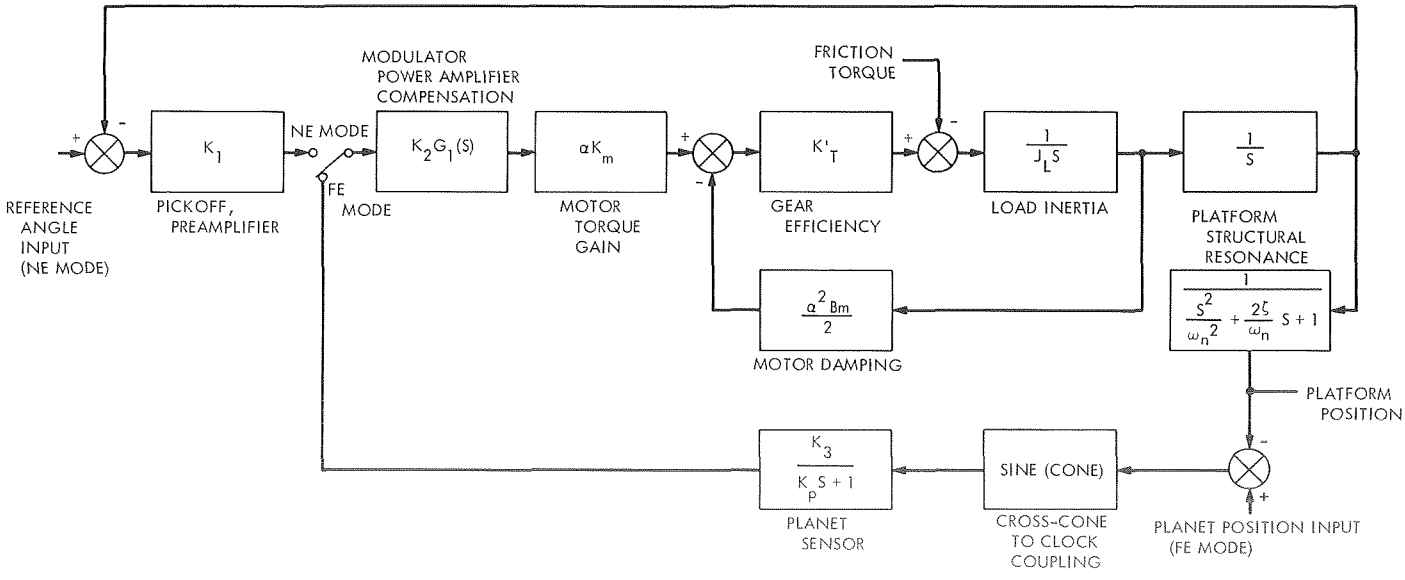

Fig. 17. Single axis representation: SCAN platform servo clock axis

The first modification from the previously developed model involves the servo motor and gear train representation. The factor K'_T has been inserted in the actuator model to account for the effective torque transmission efficiency of the gear train. The actual gear train efficiency K_T was estimated at between 30 and 50%. However, this efficiency factor applies only to the torque transmitted to the platform. Since, in the servo model, the motor inertia reflected through the gear train and platform inertia have been lumped together, an effective gear train efficiency K'_T which can be applied to the entire motor output torque was derived.

$$\alpha^2 J_m + (1/K_T)J_p = (1/K'_T)\,(\alpha^2 J_m + J_p)$$

or

$$\frac{1}{K'_T} = \frac{\alpha^2 J_m + (1/K_T)J_p}{\alpha^2 J_m + J_p}$$

A second change is that the motor damping constant has been multiplied by a factor of one-half to account for the curvature of the servo motor speed-torque curves since a low-speed motor operation is assumed for the stability analysis. Since the damping attributable to the motor is much larger than the miscellaneous damping term B_p, the constant representing the miscellaneous damping factors can be eliminated in the actuator model. Finally, the load moment of inertia of the servo has been lumped into a single term; i.e.,

$$J_L = \alpha^2 J_m + J_p$$

The moment of inertia of the platform is about 5.0 slug-ft^2. The moment of inertia of the rotor in the servo motor is about 0.76 gm-cm^2 (5.6 $\times$ 10^{-8} slug-ft^2). Increasing the effective motor moment of inertia to about 7 $\times$ 10^{-8} slug-ft^2 to account for the gear train inertias, the effective load inertia may then be calculated, as follows:

$$J_L \cong 5.0 + (27{,}000^2)\,(7)\,(10^{-8}) = 56.0 \text{ slug-ft}^2$$

In addition to actuator changes, the $G_2(S)$ function associated with the planet sensors is shown as a simple first-order lag in Fig. 17.

The parameters associated with the SCAN control system servos are listed in Table 5. Some of these parameters have already been specified, the remainder will be selected in the succeeding analysis.

Two of the basic SCAN performance requirements may be stated as:

(1) The platform slewing rate shall be greater than 1 deg/s.

(2) The maximum static error angle due to friction shall be less than 0.1 deg.

Table 5. SCAN servo parameters

Symbol	Clock, nominal	Cone, value	Definition or comments
K_1, K_4	4.2 V dc/deg	10 V dc/deg	Pickoff and preamplifier gain
K_2, K_5	4.2 V dc/deg	1.75 V rms/V dc	Modulator and power amplifier gain
K_m	2.86 (10^{-4}) ft-lb/V rms	2.86 (10^{-4}) ft-lb/V rms	Motor torque constant = stall torque/rated control winding voltage
K_T	0.4	0.4	Gear train torque transmission efficiency
α	27,034:1	27,034:1	Gear ratio
J_m	0.76 gm-cm^2	0.76 gm-cm^2	Servo motor rotor moment of inertia
J_p	4.9 $\pm$ 0.7 slug-ft^2	5.4 slug-ft^2	Platform moment of inertia
J_L	56 slug-ft^2	56 slug-ft^2	Effective load moment of inertia
B_m	3.9 (10^{-6}) ft-lb/rad/s	3.9 (10^{-6}) ft-lb/rad/s	Motor damping constant = stall torque/no load speed
ζ	0.02 to 0.1	0.02 to 0.1	Damping constant of structural resonance
T_p	0.0145 s	0.0145 s	Planet sensor time constant
Sine (cone)	0.417	—	Sine of the cone angle (145 deg $\leq$ cone angle $\leq$ 165 deg)
K_3	10 V dc/deg	10 V dc/deg	Planet sensor gain

The first of the above requirements arises out of operational considerations; in particular, when the platform clock and cone angles are slewed through a CC&S command, the slew is commanded incrementally at a 1-deg/s rate. The second requirement is derived from a consideration of SCAN system errors. The bandwidth of the SCAN platform servos does not appear critical. For example, any harmonics of spacecraft limit cycle motion with a significant amplitude have a frequency less than 0.01 Hz. In addition to these performance requirements, the SCAN platform servos should provide stable operation under all operating conditions. A phase margin greater than 50 deg and gain margin of 15 dB would appear to be reasonable goals. Finally, the SCAN servos shall be capable of operating in a predictable manner in a 1-g environment as well as a 0-g environment, since the system testing is performed at 1 g.

Examination of the block diagram of Fig. 17 shows that the error angle of the servo due to friction in the far-encounter mode may be calculated as:

$$\text{Error Angle} = \frac{T_F}{\alpha K_T K_m K_2 K_3 \text{ sine (cone)}}$$

where it is assumed that $G_1(S)$ is expressed in such a form that

$$\lim_{s \to 0} G_1(S) = 1$$

When the estimated 0-g friction of 20 in.-lb and the specified maximum error angle of 0.1 deg are substituted into this equation, a minimum required servo loop gain is obtained.

$$\alpha K_T K_m K_2 K_3 \text{ sine (cone)} \geq = 16.5 \text{ ft-lb/deg}$$

Further substituting minimum values for K_T, K_m, and α yields:

$$K_2 K_3 \text{ sine (cone)} \geq 8 \text{ V rms/deg}$$

The open loop transfer function of the far-encounter scan servo loop is taken from Fig. 17 as:

$$F(S) = \frac{2K_m K_2 K_3 \text{ sine (cone)}\ G_1(S)}{(\alpha B_m S)\left(\frac{2J_L}{\alpha^2 K'_T B_m} S + 1\right)(T_p S + 1)\left(\frac{S^2}{\omega_n^2} + \frac{2\zeta}{\omega_n} S + 1\right)}$$

Substituting previously derived nominal clock-axis values into this equation, and rearranging slightly, yields:

$$F_1(S) = \frac{(5.44 \times 10^{-3})\ K_2 K_3 \sin \text{(cone)}\ G_1(S)}{S\left(\frac{S}{22} + 1\right)\left(\frac{S}{69} + 1\right)\left(\frac{S^2}{\omega_n^2} + \frac{2\zeta}{\omega_n} S + 1\right)}$$

A Bode plot of this function for $\omega_n = 2\pi\ (6)$, $\zeta = 0.02$ (which may be seen to be the worst case), $G_1(S) = 1$, and $K_2 K_3 \text{ sine (cone)} = 17.5 \dfrac{\text{V rms}}{\text{deg}}$ is presented in Fig. 18.

The uncompensated [$G_1(S) = 1$] servo loop design in Fig. 18 has about 72 deg phase margin, but the gain margin is essentially 0. If the structural resonance were excluded from the transfer function, the frequency at which the phase of the resultant transfer function reaches −180 deg is almost exactly the same as the projected minimum structural resonant frequency of 6 Hz. Hence, it appears that the design point represented in Fig. 18 would produce extremely marginal performance.

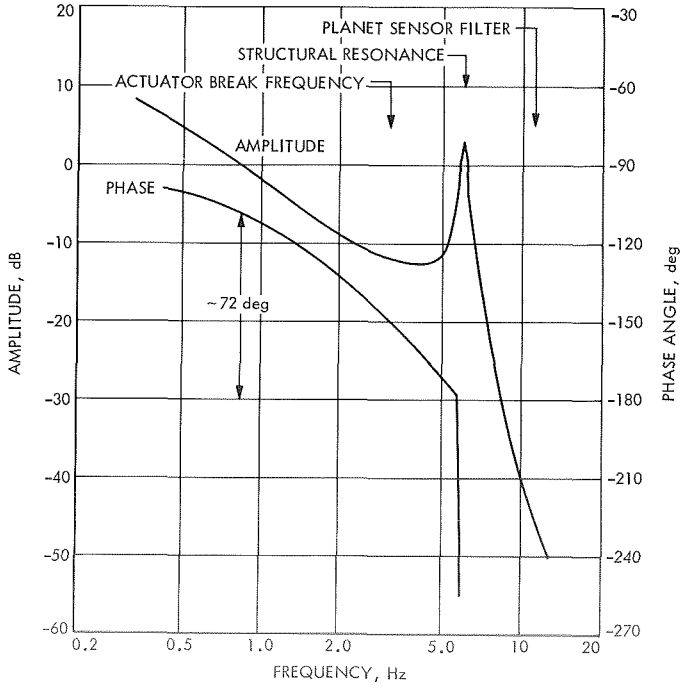

Fig. 18. Bode plot, uncompensated *FE* loop

A significant improvement in the stability margins of the platform control servos can be obtained by inserting a first-order lag in the servo loop at approximately the same frequency as the minimum structural resonant frequency; i.e.,

$$G_1(S) = \frac{1}{\frac{S}{2\pi 6} + 1}$$

The Bode plot which results when this compensation network is used is shown in Fig. 19. The stability margins associated with the compensated *FE* servo loop are shown to be about 14 dB in gain and 62 deg in phase margin. A root locus plot of the same function is shown in Fig. 20. The loop gain at which the system is operated is indicated on each locus. From this it can be seen that the −3 dB closed loop bandwidth is about 10.6 rad/s (1.7 Hz) and damping ratio (cosine θ) is about 0.82.

The cone angle range for the SCAN platform *FE* mode is 145–165 deg. Hence the sine (cone) term may be calculated as 0.417 ±0.158. The gain of the two planet sensors was selected at 10 V dc/deg to alleviate noise problems in the signal transmission. The required

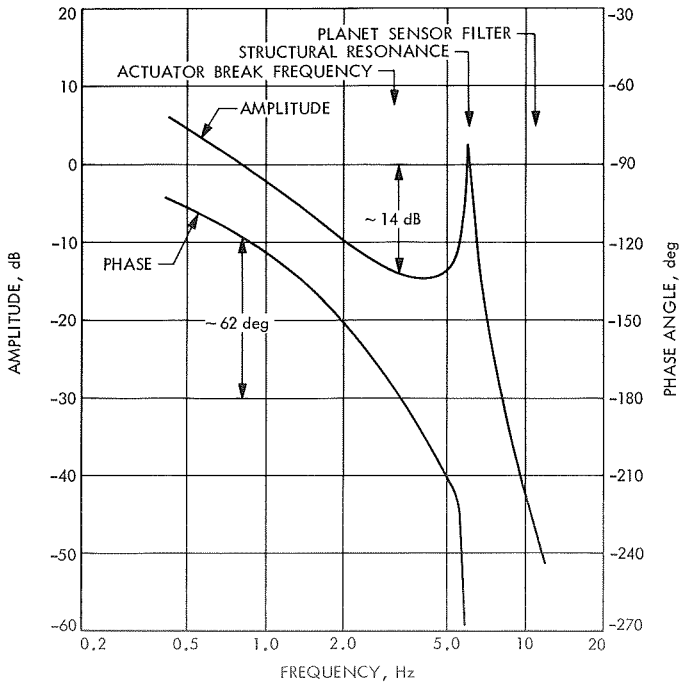

Fig. 19. Bode plot, compensated *FE* loop

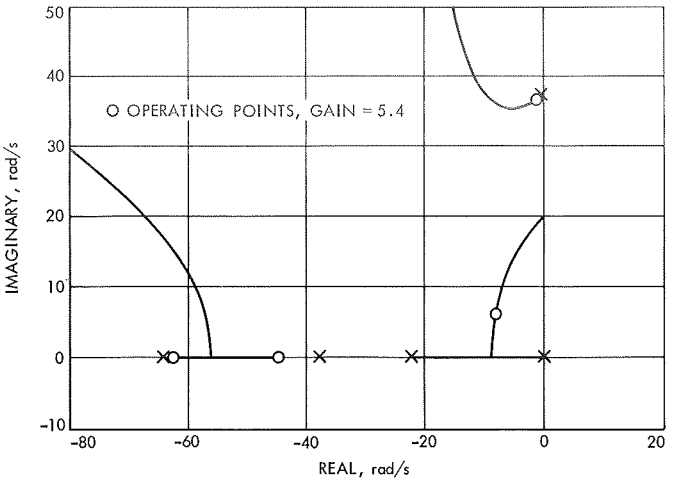

Fig. 20. Root locus plots, compensated *FE* servo loop

electronic gain of the modulator and power amplifier in the SCAN servos may, therefore, be calculated as:

$$K_2 = \frac{17.5 \text{ V rms/deg}}{K_3 \sin (\text{cone})}$$

$$\text{clock axis } K_2 = \frac{17.5 \text{ V rms/deg}}{10\,(0.417) \text{ V dc/deg}} = 4.2 \text{ V rms/V dc}$$

$$\text{cone axis } K_5 = \frac{17.5 \text{ V rms/deg}}{10 \text{ V dc/deg}} = 1.75 \text{ V rms/V dc}$$

The *NE* open-loop transfer function of the servo system of Fig. 17 differs from the *FE* case only in that the structural resonance no longer has any effect, and the pickoff and preamplifier gain must be used in place of the planet sensor. The transfer function is:

$$F_2(S) = \frac{5.44\,(10^{-3})\,K_1K_2G_1(S)}{S(S/22 + 1)}$$

Inserting the previously derived compensation, and assuming the same gain (K_1K_2 = 17.5 V dc/deg) then yields:

$$F_2(S) = \frac{5.44}{S(S/22 + 1)\,(S/37.7 + 1)}$$

A Bode plot for this transfer function is shown in Fig. 21. The 19-dB gain and 72 deg phase stability margins afforded by the design point shown in this figure should be adequate to assure proper servo loop operation under all possible conditions.

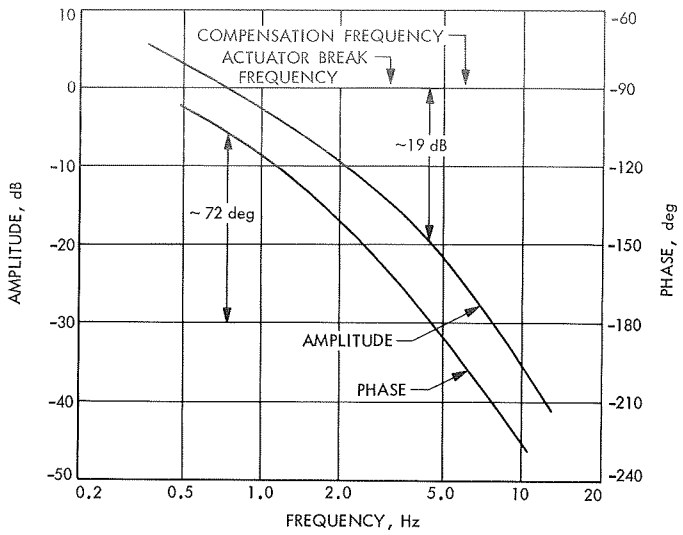

Fig. 21. Bode plot, compensated *NE* loop

The gain of the modulator and power amplifier was previously specified as 4.2 V rms/V dc in the clock axis and 1.75 V rms/V dc in the cone axis. The required preamplifier and pickoff gain may then be calculated as:

$$\text{clock axis, } K_1 = \frac{17.5 \text{ V rms/deg}}{4.2 \text{ V rms/V dc}} = 4.17 \text{ V dc/deg}$$

$$\text{cone axis, } K_4 = \frac{17.5 \text{ V rms/deg}}{1.75 \text{ V rms/V dc}} = 10 \text{ V dc/deg}$$

The potentiometers which are used as a pickoff in both axes provide a sensitivity of 4.6×10^{-2} V dc/deg. Hence, the required clock preamplifier gain is 220.

As a part of the SCAN platform servo design, a parameter variation analysis was undertaken. This parameter variation analysis considered the effects of possible worst-case tolerance combinations on the performance and stability of the SCAN platform control servos. The tolerance ranges which were considered are listed in Table 5. The tolerance analysis considered primarily the *FE* operating mode, since the stability margins are less in this mode.

A summary of the parameter variation analysis is presented in Fig. 22 and Table 5. The Table 6 presents the nominal, maximum, and minimum calculated values for both performance and stability criteria. In general, the tolerances on the following parameters were found to have the most pronounced effect on the servo performance.

(1) *FE* cone angle.

Table 6. SCAN servo parameter variations, *FE* mode

Parameter	Nominal	Maximum	Minimum
Gain margin, dB	14	20	8
Phase margin, deg	62	80	45
Bandwidth (−3 dB), Hz	1.7	2.3	0.8
Platform slewing rate			
0-g loading (20 in.-lb), deg/s	1.47	1.56	1.36
1-g loading (100 in.-lb), deg/s	1.14	1.31	0.89
Static stiffness, in.-lb/deg	645	1164	308
Static error angle (friction)			
0-g (20 in.-lb), deg	0.031	0.068	0.016
1-g (100 in.-lb), deg	0.16	0.34	0.08
Stall torque (slip clutch), in.-lb	300	325	275

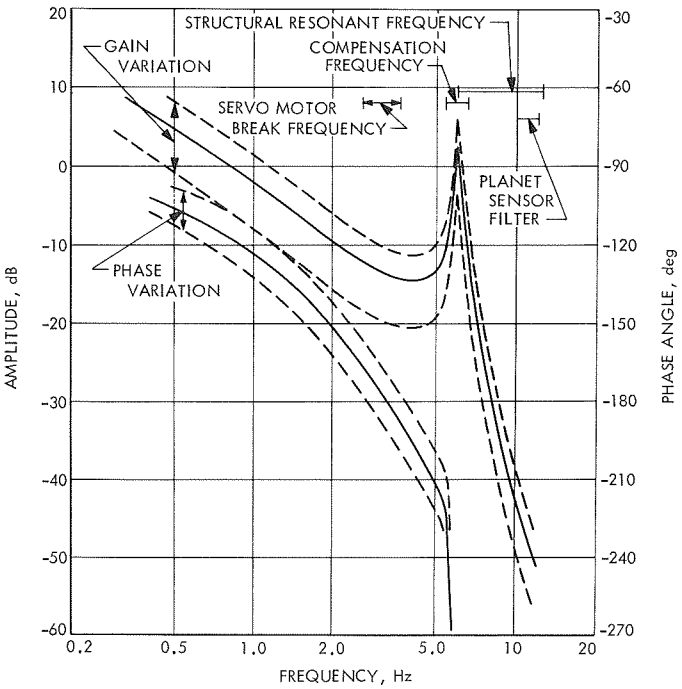

Fig. 22. Bode plot, *FE* servo parameter-variation analysis

(2) Planet sensor gain.

(3) Servo motor damping constant.

(4) Servo motor torque constant.

4. SCAN servo electronics. The circuit configuration which was developed to meet the SCAN servo electronics requirements is shown in Fig. 23, and a servo electronic assembly (clock and cone axes) is shown in Fig. 24. As illustrated, extensive use is made of the

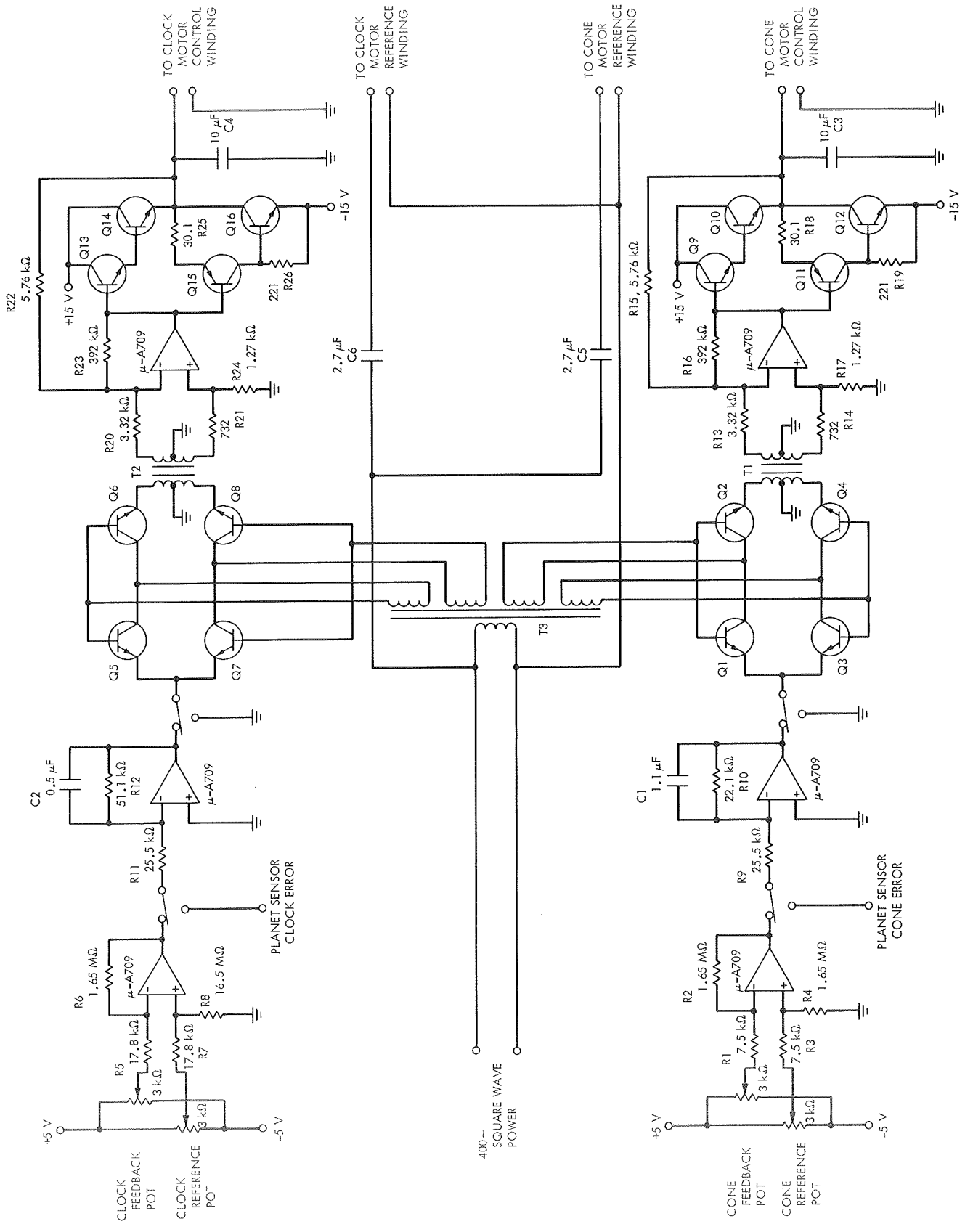

Fig. 23. SCAN servo electronics

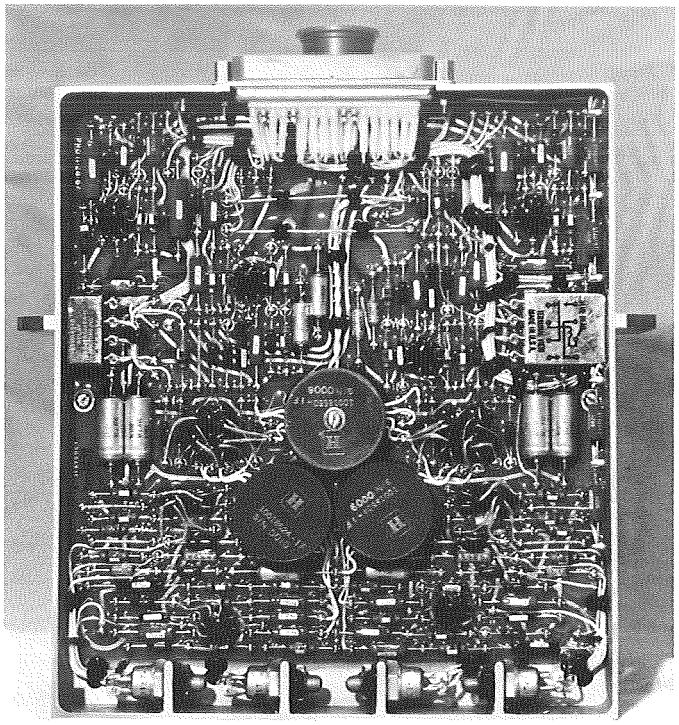

Fig. 24. SCAN servo drive amplifiers subassembly

μ-A709 analog integrated circuit amplifier. This amplifier provides low drift, small package size, and high-voltage gain. Such auxiliary circuit elements as shaping or biasing networks and over-voltage or short-circuit protection elements are not shown in Fig. 23. Only the electronic elements necessary to explain the basic circuit functions are included.

The input potentiometers (feedback and reference potentiometers) to each channel of electronics are connected to ± 5 V supplies with no center tapped ground reference. The outputs are then connected into a differential amplifier so that servo null is achieved when the two input voltages are identical. This arrangement minimizes the effects of power supply variations. Differences between the two inputs at corresponding potentiometer positions is primarily a function of potentiometer linearity, potentiometer resolution, and unequal loading of the two potentiometers by the differential amplifier.

The source impedance seen by the differential amplifier input circuits varies from near 0 to 750 Ω. The high- and balanced-input impedance of the differential amplifier, along with the low-input potentiometer impedance, maintain the potentiometer non-linearity due to loading below 0.3%; the loading unbalance is practically negligible.

The first μ-A709 unit in each electronics channel is operated as a differential amplifier to minimize common mode errors. Common mode rejection afforded by the μ-A709 amplifier is approximately 70 dB. The positive and negative gains of the differential amplifiers are also compensated to be equal. For the cone axis configuration shown in Fig. 23, the negative gain is R_2/R_1. The positive gain is given by $(1 + R_2/R_1)\ (R_4/(R_3 + R_4))$. Selecting $R_1 = R_3$ and $R_2 = R_4$ makes the two gain expressions equal, and also makes the input impedance to the two differential amplifier inputs identical. The nominal differential amplifier gain is therefore calculated as 92.7 in the clock axis channel and 220 in the cone axis channel.

The gain accuracy and gain stability of the differential amplifiers are affected by such factors as resistor tolerances, temperature coefficients, source resistance, and finite loop gain. The maximum gain deviation is between $+3$ and -4% under all conditions. Assuming the minimum forward gain for the μ-A709, over 40 dB of feedback is provided for the highest closed-loop gain. The calculated maximum, worst case, offset voltage referred to the input is approximately ± 8.5 mV.

The second μ-A709 amplifier in each channel provides the proper voltage gain to close the servo loops through either the planet sensor or the input potentiometers and differential amplifiers. The gain of these stages, calculated as the ratio of the feedback resistor to the input resistor, is 2.0 in the clock channel and 0.87 in the cone channel. The required lag compensation in each channel is implemented using R10 and C1 (or R_{12} and C2) in the feedback network of this amplifier. The break frequency in each axis is set for about 6.3 Hz.

The two modulators and power amplifiers are identical, hence only the cone channel will be discussed. Transistors Q1 through Q4 provide full wave modulation of the second amplifier output. Since the input 400-Hz signal is a square wave, and since no filtering is used, the modulator output is also a square wave. Modulator drive is obtained through a transformer T3. The collector-to-base drive is used in the modulators to minimize offset voltage in the on-mode. The modulated signal is fed to the power amplifier through a coupling transformer T1. The primary-to-secondary turns ratio in the transformer is 2:1; therefore, the gain from the output of the second μ-A709 amplifier to the differential input voltage of the power amplifier is approximately 1 V rms/V dc input (400-Hz square wave). Since only the fundamental

of this 400-Hz square wave is useful in driving the servo motor, and since the rms value of the fundamental component of the square wave is about 0.9 of the square wave maximum value, the effective gain across the modulator and coupling transformer is about 0.9.

Each power amplifier uses a μ-A709 amplifier and four transistors in a Darlington configuration. The R_{16} and R_{13} form a local feedback loop around the μ-A709 unit to provide a low-drive impedance for the output stage. The overall power amplifier gain is determined by R_{15}, R_{13}, R_{14}, and R_{17}. The gain from the coupling transformer secondary to the output is given by:

$$\text{Gain} = \tfrac{1}{2}\left[\frac{R_{15}}{R_{13}} + \left(1 + \frac{R_{15}}{R_{13}}\right)\left(\frac{R_{17}}{R_{14} + R_{17}}\right)\right]$$

This gain may be calculated as 1.72. The values of R_{14} and R_{17} (relative to R_{13} and R_{15}) are chosen to keep the gain balanced in the positive and negative differential amplifier channels and to maintain equal loading on the two halves of the coupling transformer secondary. These criteria require that R_{14} and R_{17} satisfy the following relationships:

$$\frac{R_{15}}{R_{13}} = \frac{R_{17}}{R_{14}}$$

and

$$R_{14} + 2R_{17} = R_{13}$$

The power amplifier operates in the class B mode for efficiency. The output wave form is nominally a square wave. The servo-motor control winding is center-tapped; the two halves are driven in parallel. The nominal 400-Hz sine wave rating for the parallel connection is 10 V rms.

Phase shift capacitors (C5 and C6) are used to shift the phase of the servo-motor reference winding excitation and obtain the required 90 deg phase relationship between reference winding and control winding signals. These phase shift capacitors are, of course, effective for only the fundamental of the square-wave drive signals.

C. SCAN Control System Error Analysis

1. Far-encounter mode. The SCAN control system errors in the *FE* mode are relatively simple. Since the pointing is closed through the line-of-sight to the planet with a planet sensor, errors such as gear train backlash and mechanical alignments have a negligible effect on the accuracy of the SCAN control system. The only two errors which contribute to the control system pointing accuracy are errors in the servo loop and errors in the planet sensor. These error sources are briefly discussed.

a. Far-encounter servo errors. Any servo error which results in an offset between the line-of-sight to the planet and the planet sensor line-of-sight will cause an error in the *FE* mode. Such errors as amplifier null stability, bearing or gear train stiction, and servo-motor starting voltage must therefore be considered. The scale factor of the planet sensor error signal is high enough, 10 V/deg, so that the maximum null offset in the servo electronics 8.5 mV will cause a negligible error. The maximum servo error in either axis due to bearing friction is estimated at 0.06 deg. The starting voltage for the actuators has been measured at less than 1 V rms. This 1-V error corresponds to a maximum pointing error of 0.06 deg.

b. Planet sensor errors. The maximum (two axes) null error for the planet sensor is specified as 0.20 deg. In order to meet this performance, the null errors in each of the two orthogonal planet-sensor sensitive axes are limited to 0.14 deg maximum. This null error includes the original alignment and calibration of the instrument plus all of the optics and electronics shifts which contribute to the null instability of the planet sensor.

The *FE* SCAN control system errors are listed in Table 7. As shown, the cone axis errors result directly in platform line-of-sight errors. The clock axis servo errors, however, do not directly result in cross-cone line-of-sight errors since the platform line-of-sight is not normal to the clock axis. The clock axis errors must be multiplied by the sine of the cone angle in calculating the resulting cross-cone line-of-sight error. A root-sum-square is used to calculate the total cone and cross-cone errors. The

Table 7. SCAN control system *FE* errors

Error source	Error magnitude, deg, 3σ	Line-of-sight errors, deg, 3σ	
		Cone, deg, 3σ	Cross-cone, deg, 3σ
Servo errors:			
Friction hangoff angle	$\pm$0.06	0.06	0.034
Actuator starting voltage	$\pm$0.06	0.06	0.034
Planet sensor null accuracy	$\pm$0.14	0.14	0.14
	Total	0.164	0.148

maximum *FE* line-of-sight error, calculated as the root-sum-square of the two orthogonal errors in Table 7 is 0.22 deg. This accuracy is compatible with the required SCAN control system *FE* pointing accuracy of 0.25 deg.

2. Near-encounter mode. In the *NE* mode, the two performance parameters of interest are the aiming resolution and the readout accuracy of the platform. The aiming resolution is limited by the minimum angle with which the open loop pointing direction can be changed to ± 0.5 deg.

The readout accuracy of the SCAN control system refers to the precision with which the pointing direction of the platform can be determined through the spacecraft telemetry readings. The platform pointing direction relative to a space-fixed coordinate system is ultimately necessary. Hence, both the accuracy of the platform readout with respect to the spacecraft coordinate system and the motion of the spacecraft coordinate system (due to the limit cycle motion of the attitude control system) must be considered in an overall error analysis. Only the accuracy of the platform readout with respect to the spacecraft coordinate system, however, is documented in this report.

The error sources which limit the SCAN platform readout accuracy are listed in Table 8. The total line-of-sight (LOS) errors shown in Table 8 yield the desired SCAN platform readout accuracy of ± 0.20 deg/axis.

The geometric relationship between the clock axis and cross-cone axis must again be considered. Such clock errors as gear backlash and readout interpolation must be multiplied by the sine of the cone angle in order to obtain the resulting cross-cone error. A cone angle of 145 deg was assumed for the calculations of Table 8. Non-Gaussian distributions were also assumed for some of the errors. The errors were then combined considering the form of the probability density functions. The sum of the second moments of the individual distributions was taken to be equal to the variance of the combined probability density.

Table 8. Maximum SCAN platform readout errors

Error source	Error magnitude, deg	LOS errors, deg	
		Cone	Cross-cone
Readout resolution	± 0.018[a]	± 0.018	± 0.014
Readout calibration	± 0.050[b]	± 0.050	± 0.050
Readout interpolation	± 0.050[c]	± 0.050	± 0.038
Gear backlash	± 0.080[a]	± 0.080	± 0.061
Structural alignment stability	± 0.10[b]	± 0.10	± 0.10
	Total	± 0.19	± 0.12

[a]Error assumed to have a rectangular distribution.

[b]Error assumed to have a Gaussian distribution.

[c]Error assumed to have a triangular distribution.

a. Readout resolution. Both the clock and cone axis platform positions are monitored using the spacecraft telemetry readout. Two potentiometers are geared to each platform axis. The coarse potentiometer rotates at about 1.6 × platform speed; the fine potentiometer rotates at about 80 × platform speed. Each potentiometer is encoded in the telemetry system to a resolution of 1 part in 127. The readout resolution associated with this readout scheme is therefore nominally ± 0.018 deg.

b. Readout calibration. Mechanical tolerances necessitate a calibration of the SCAN platform readout after a spacecraft is assembled. The calibration is accomplished by obtaining data at a limited number of platform orientations, representative of the expected operating positions, and then using linear interpolation to bridge the gaps between calibration points. The calibration procedure is designed to provide a maximum error of ± 0.05 deg for any data point.

c. Readout interpolation. The assumed linear interpolation procedure has the potential to contribute additional readout errors. The errors contributed by the linear interpolation process was estimated to be a maximum of ± 0.05 deg.

d. Gear backlash. Anti-backlash gears are used in the 80:1 gear train between the platform and the fine potentiometer to limit the backlash errors in the gear train. The backlash in this gear train, along with any potentiometer wiper hysteresis, is expected to cause a readout error at the platform axis of less than ± 0.08 deg.

e. Structural alignment stability. The platform readout technique is critically dependent on the structural stability between the basic spacecraft coordinate system and the platform LOS. The structural stability errors here are intended to include both changes in the structure, e.g., creep, and clearance tolerances, e.g., bearing clearances. This error must be limited to about a ± 0.10 deg magnitude per axis in order to obtain the desired SCAN platform readout performance.

NASA — JPL — Comt., L.A., Calif.

N71-14366

TECHNICAL REPORT STANDARD TITLE PAGE

1. Report No. 32-1506	2. Government Accession No.	3. Recipient's Catalog No.
4. Title and Subtitle MARINER MARS 1969 SCAN CONTROL SUBSYSTEM DESIGN AND ANALYSIS		5. Report Date October 30, 1970 6. Performing Organization Code
7. Author(s) T. Kerner, H. H. Horiuchi		8. Performing Organization Report No.
9. Performing Organization Name and Address JET PROPULSION LABORATORY California Institute of Technology 4800 Oak Grove Drive Pasadena, California 91103		10. Work Unit No. 11. Contract or Grant No. NAS 7-100 13. Type of Report and Period Covered Technical Report
12. Sponsoring Agency Name and Address NATIONAL AERONAUTICS AND SPACE ADMINISTRATION Washington, D.C. 20546		14. Sponsoring Agency Code

15. Supplementary Notes

16. Abstract

The SCAN platform control system designed for the Mariner Mars 1969 spacecraft is described. The platform, which acts as a mounting base for the science instruments, has two deg-of-freedom about a set of spacecraft fixed coordinates. The system controls the platform movement and position. This report covers the detailed system design, the servo analysis, and the system error analysis.

17. Key Words (Selected by Author(s))	18. Distribution Statement
Control and Guidance Mariner Mars 1969 Project	Unclassified -- Unlimited

19. Security Classif. (of this report)	20. Security Classif. (of this page)	21. No. of Pages	22. Price
Unclassified	Unclassified	22	

HOW TO FILL OUT THE TECHNICAL REPORT STANDARD TITLE PAGE

Make items 1, 4, 5, 9, 12, and 13 agree with the corresponding information on the report cover. Use all capital letters for title (item 4). Leave items 2, 6, and 14 blank. Complete the remaining items as follows:

3. Recipient's Catalog No. Reserved for use by report recipients.

7. Author(s). Include corresponding information from the report cover. In addition, list the affiliation of an author if it differs from that of the performing organization.

8. Performing Organization Report No. Insert if performing organization wishes to assign this number.

10. Work Unit No. Use the agency-wide code (for example, 923-50-10-06-72), which uniquely identifies the work unit under which the work was authorized. Non-NASA performing organizations will leave this blank.

11. Insert the number of the contract or grant under which the report was prepared.

15. Supplementary Notes. Enter information not included elsewhere but useful, such as: Prepared in cooperation with... Translation of (or by)... Presented at conference of... To be published in...

16. Abstract. Include a brief (not to exceed 200 words) factual summary of the most significant information contained in the report. If possible, the abstract of a classified report should be unclassified. If the report contains a significant bibliography or literature survey, mention it here.

17. Key Words. Insert terms or short phrases selected by the author that identify the principal subjects covered in the report, and that are sufficiently specific and precise to be used for cataloging.

18. Distribution Statement. Enter one of the authorized statements used to denote releasability to the public or a limitation on dissemination for reasons other than security of defense information. Authorized statements are "Unclassified—Unlimited," "U. S. Government and Contractors only," "U. S. Government Agencies only," and "NASA and NASA Contractors only."

19. Security Classification (of report). NOTE: Reports carrying a security classification will require additional markings giving security and downgrading information as specified by the Security Requirements Checklist and the DoD Industrial Security Manual (DoD 5220.22-M).

20. Security Classification (of this page). NOTE: Because this page may be used in preparing announcements, bibliographies, and data banks, it should be unclassified if possible. If a classification is required, indicate separately the classification of the title and the abstract by following these items with either "(U)" for unclassified, or "(C)" or "(S)" as applicable for classified items.

21. No. of Pages. Insert the number of pages.

22. Price. Insert the price set by the Clearinghouse for Federal Scientific and Technical Information or the Government Printing Office, if known.